Mon. Not. R. Astron. Soc. **000**, 1–6 (2007) Printed 16 October 2008 (MN LATEX style file v2.2)

Dark matter halo concentrations in the *Wilkinson Microwave Anisotropy Probe* year 5 cosmology

Alan R. Duffy[1,2], Joop Schaye[2], Scott T. Kay[1] and Claudio Dalla Vecchia[2]
[1] *Jodrell Bank Centre for Astrophysics, Alan Turing Building, The University of Manchester, M13 9PL, U.K.*
[2] *Leiden Observatory, Leiden University, PO Box 9513, 2300 RA Leiden, The Netherlands*

16 October 2008

ABSTRACT

We use a combination of three large N-body simulations to investigate the dependence of dark matter halo concentrations on halo mass and redshift in the *Wilkinson Microwave Anisotropy Probe* year 5 (WMAP5) cosmology. The median relation between concentration and mass is adequately described by a power-law for halo masses in the range $10^{11} - 10^{15}\,h^{-1}\mathrm{M}_{\odot}$ and redshifts $z < 2$, regardless of whether the halo density profiles are fit using NFW or Einasto profiles. Compared with recent analyses of the Millennium Simulation, which uses a value of σ_8 that is higher than allowed by WMAP5, $z = 0$ halo concentrations are reduced by factors ranging from 23 per cent at $10^{11}\,h^{-1}\mathrm{M}_{\odot}$ to 16 per cent at $10^{14}\,h^{-1}\mathrm{M}_{\odot}$. The predicted concentrations are much lower than inferred from X-ray observations of groups and clusters.

Key words: galaxies: clusters: general – galaxies: haloes – cosmological parameters – dark matter – cosmology: theory – methods: N-body simulations

1 INTRODUCTION

Investigations into dark matter (hereafter DM) clustering and dynamics have progressed greatly thanks to large-scale cosmological simulations run with the aid of supercomputers. In particular, the N-body technique has allowed us to follow the detailed hierarchical build-up of virialised DM structures, resulting in near spherical haloes that are well described by the Navarro, Frenk & White profile (Navarro et al. 1997, hereafter NFW). The NFW density profile is described by just two parameters, the concentration, c, and the total mass, M, of the halo. Simulations have shown that these two parameters are correlated, with the average concentration of a halo being a weakly decreasing function of mass (e.g. NFW; Bullock et al. 2001; Eke et al. 2001, hereafter ENS; Shaw et al. 2006; Maccio et al. 2007). Observations of galaxy groups and clusters using X-ray and gravitational lensing data are being used to test this hypothesis and generally confirm the anti-correlation between c and M (e.g. Buote et al. 2007; Schmidt & Allen 2007), although the concentrations inferred from strong gravitational lensing may exceed those predicted by the simulations (e.g. Hennawi et al. 2007; Broadhurst & Barkana 2008).

The best statistical constraints on the halo concentration distribution currently come from the `Millennium Simulation` (Springel et al. 2005), hereafter `MS`, in which 2160^3 DM particles were allowed to interact gravitationally in a cosmological box of length $500\,h^{-1}$Mpc. The resulting $c(M)$ relation is well described by a power law, $c \propto \mathrm{M}^{-0.1}$ (Neto et al. 2007, hereafter N07). The `MS` used cosmological parameters from the *Wilkinson Microwave Anisotropy Probe* year 1 (WMAP1) data release (Spergel et al. 2003) combined with constraints from the Two Degree Field Galaxy Redshift Survey (Percival et al. 2001), henceforth referred to as the WMAP1 cosmology.

In this letter, we use a set of N-body simulations to quantify the relation between concentration and mass in the more recent WMAP year 5 cosmology (Komatsu et al. 2008), henceforth WMAP5, in which the most significant change from WMAP1 is a downward shift in σ_8 by around 13 per cent. Because the $c(M)$ relation is very sensitive to the primordial power spectrum (e.g. ENS; Alam, Bullock, & Weinberg 2002; Dolag et al. 2004; Kuhlen et al. 2005), it is not clear whether the `MS` results accurately describe our Universe. Indeed, we will show that the WMAP5 cosmology results in a significant decrease in both the slope and the normalisation of the $c(M)$ relation. While this reduction in halo concentrations may make it easier for models of galaxies to match observations (e.g. van den Bosch, Mo, & Yang 2003; Gnedin et al. 2007), we will show that it results in strong disagreement between simulations and X-ray observations of groups and clusters of galaxies.

2 SIMULATIONS

We analyse a set of three N-body simulations, run using GADGET2 (Springel 2005). Each simulation contains 512^3

DM particles but with a progressively larger comoving box size: 25, 100, and 400 h^{-1}Mpc for runs *L025*, *L100* and *L400*, respectively. By combining the results of the three simulations, we cover four orders of magnitude in halo mass, a range that exceeds that of N07, although our total number of haloes is smaller than in the MS. Our highest resolution simulation (*L025*) uses a Plummer-equivalent comoving softening of 2 kpc/h, with a maximum proper value of 0.5 kpc/h, reached at $z = 3$; *L100* and *L400* have values 4 and 16 times larger respectively. The particle masses are $8.34\times10^6\,h^{-1}\mathrm{M}_\odot$, $5.33\times10^8\,h^{-1}\mathrm{M}_\odot$ and $3.41\times10^{10}\,h^{-1}\mathrm{M}_\odot$, for *L025*, *L100* and *L400*, respectively.

Glass-like cosmological initial conditions were generated at redshift $z = 127$ using the Zeldovich approximation and a transfer function generated using CMBFAST (v. 4.1, Seljak & Zaldarriaga 1996). We use the WMAP5 (CMB only) cosmology, with $[\Omega_m, \Omega_b, \Omega_\Lambda, h, \sigma_8, n_s]$ given by [0.258, 0.0441, 0.742, 0.719, 0.796, 0.963]. For comparison, the MS used the WMAP1 cosmology, [0.25, 0.045, 0.75, 0.73, 0.9, 1.0]; for which the value of σ_8 is about 13 per cent larger.

2.1 Halo definitions and density profiles

Halo virial masses and radii are determined using a spherical overdensity routine within the SUBFIND algorithm (Springel et al. 2001) centred on the main subhalo of Friends-of-Friends (FOF) haloes (Davis et al. 1985).

We perform all calculations for three different halo definitions, which all take the halo centre to be the location of the most bound particle in the FOF group. According to the first definition, which is motivated by the spherical top-hat collapse model, a halo consists of all matter within the radius $r_{\rm vir}$ for which the mean internal density is Δ times the critical density $\rho_{\rm crit} = 3H^2/8\pi G$, where Δ depends on both cosmology and redshift and is given by Bryan & Norman (1998). Using the second (third) definition, a halo consists of all matter within the radius r_{200} ($r_{\rm mean}$) for which the mean internal density is 200 times the critical (mean background) density. Note that NFW adopted the second definition. We will use $M_{\rm vir}$, M_{200}, and $M_{\rm mean}$ to denote the corresponding halo masses.

Two different density profiles (NFW and Einasto) are fit to well-resolved haloes using a procedure which closely follows N07. For each halo with at least 10^4 particles within $r_{\rm vir}$, all particles in the range $-1.25 \leqslant \log_{10}(r/r_{\rm vir}) \leqslant 0$ are binned radially in equally spaced logarithmic bins of size $\Delta \log_{10} r = -0.078$. Density profiles are then fit to these bins by minimising the difference between the logarithmic densities of the model and the data, assuming equal weighting. Haloes are only used if the convergence radius, as proposed by Power et al. (2003), is within the minimum fit radius of 0.05 $r_{\rm vir}$. The convergence radius is defined such that the two-body dynamical relaxation timescale of the particles internal to this point is similar to the age of the universe. The best-fit density profiles are used to define the halo radii, with the corresponding masses found by integrating the profiles to these radii.

We consider two samples. Our default sample contains all haloes that satisfy our resolution criteria while our 'relaxed' sample retains only those haloes for which the separation between the most bound particle and the centre of mass of the FOF halo is smaller than $0.07r_{\rm vir}$. Note that N07 found that this simple criterion resulted in the removal of the vast majority of unrelaxed haloes and as such we do not use their additional criteria. At $z = 0$ our default and relaxed samples contain 1269 and 561 haloes in total.

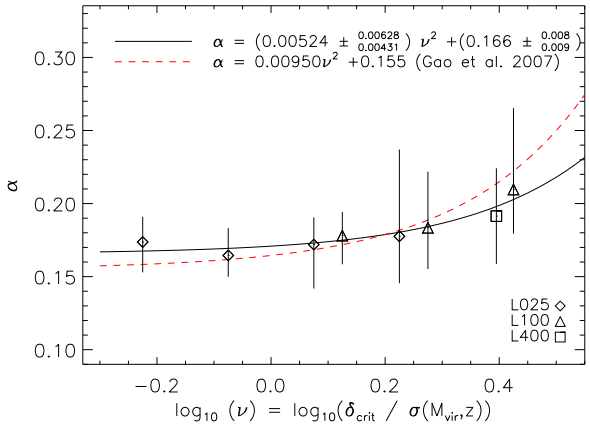

Figure 1. The relation between the Einasto power-law index α and the peak height parameter ν for stacks of haloes of our default sample. Data from redshifts $z = 0, 1$ and 2 was combined. Data points correspond to medians and error bars indicate quartiles. The solid curve is the best-fit quadratic function, whereas the dashed curve is the result from G07. The parameters for both fits are given in the legend together with the errors (68.2 per cent confidence level) obtained by bootstrap resampling the haloes.

The NFW density profile is given by

$$\rho(r) = \rho_{\rm crit}\frac{\delta_{\rm c}}{(r/r_{\rm s})(1+r/r_{\rm s})^2}\,, \qquad (1)$$

where $\delta_{\rm c}$ is a characteristic density contrast and $r_{\rm s}$ is a scale radius. The concentration is defined as $c_{200} \equiv r_{200}/r_{\rm s}$. NFW profiles were fit using the two parameters $r_{\rm s}$ and $\delta_{\rm c}$.

The Einasto profile is a rolling power-law first introduced to describe the distribution of old stars in the Milky Way. It takes the form

$$\frac{{\rm d}\ln\rho}{{\rm d}\ln r} = -2\left(\frac{r}{r_{-2}}\right)^{\alpha}\,, \qquad (2)$$

where r_{-2} is the radius at which the logarithmic slope of the density is isothermal (i.e. -2), analogous to $r_{\rm s}$ in the NFW profile. As a result the concentration, $c_{200} \equiv r_{200}/r_{-2}$, is close to the NFW value. Integrating Eq. 2 gives

$$\ln(\rho/\rho_{-2}) = -\frac{2}{\alpha}\left[(r/r_{-2})^{\alpha} - 1\right]\,, \qquad (3)$$

where ρ_{-2} is the density at r_{-2}. Gao et al. (2007, hereafter G07) have shown that there exists a simple relation between α and ν, the dimensionless 'peak-height' parameter[1], independent of redshift. We check this result for our simulations by performing a three-parameter fit to profiles averaged over ten haloes (to remove the effects of substructure). As shown in Fig. 1, our results are in agreement with G07; we therefore adopt their $\alpha(\nu)$ relation to reduce the model to two free parameters (ρ_{-2} and r_{-2}).

[1] The peak height is defined to be $\nu \equiv \delta_{\rm crit}/\sigma(M_{\rm vir}, z)$, where $\delta_{\rm crit} = 1.686$ is the linear density collapse threshold at the present

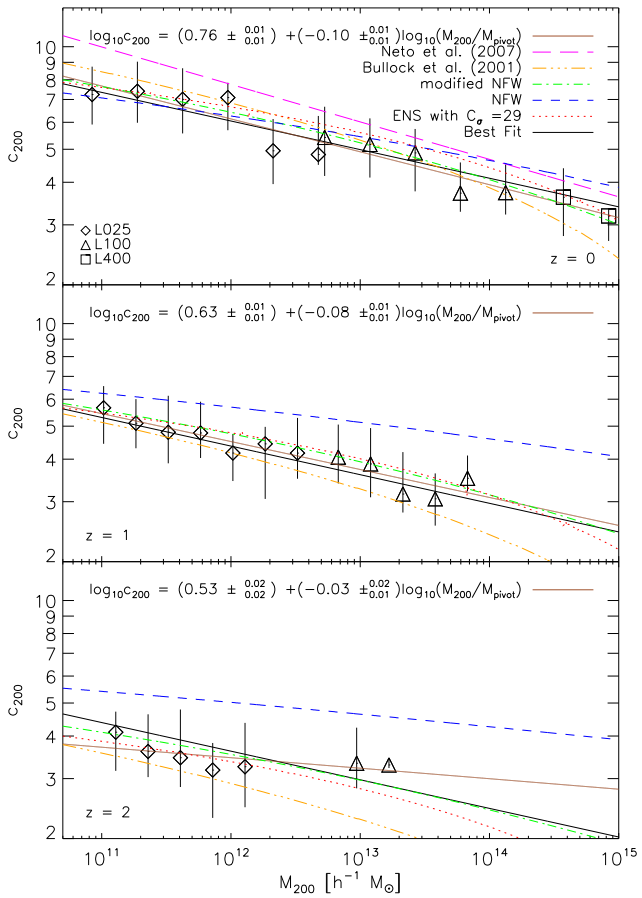

Figure 2. Concentration-mass relations for $z = 0$ (top), 1 (middle) and 2 (bottom) using NFW density profiles. Data points correspond to median values and error bars to quartiles. Only bins containing at least 5 haloes are shown. The black, solid lines show the best-fit power-law relation. The errors on the best-fit parameters, given in the legend, are determined by bootstrap resampling the haloes and correspond to 68.2 per cent confidence limits. The pink dashed line in the top panel shows the best-fit power-law relation to all haloes from N07. The other curves represent the prescriptions discussed in section 3.1. The brown solid lines correspond tothe special case where we set $C = 0$ in Eq. 4, and fit a power-law to the data at each individual redshift.

3 RESULTS

Fig. 2 shows the median $c_{200}(M_{200}, z)$ relation for $z = 0$, 1 and 2 (top, middle and bottom panels, respectively) using NFW density profiles. The data, which spans four orders of magnitude in mass and a redshift range $z = 0 - 2$ are well described by a function of the form

$$c = A(M/M_{\rm pivot})^B(1+z)^C. \quad (4)$$

The black solid line indicates the best-fit relation of this form to the data. The parameter values and errors are given in Table 1 for three different halo definitions, for both NFW and Einasto profiles, for the full and relaxed samples, and for both $z = 0$ (in which case we set $C = 0$) and $z = 0$–2.

day and $\sigma(M_{\rm vir}, z)$ is the linear *rms* density fluctuation at redshift z in a sphere containing a mass $M_{\rm vir}$.

All fits use $M_{\rm pivot} = 2\times10^{12}\,h^{-1}{\rm M}_\odot$, the median halo mass, in order to minimise the covariance between A and B.

Concentration is a decreasing function of both mass and redshift, regardless of the model density profile and halo definition that is used. We note that at high redshift, $z = 2$, the mass dependency is significantly reduced (see also Zhao et al. 2003). Compared with NFW concentrations, Einasto concentrations decrease significantly more rapidly with both mass and redshift. At $z = 0$ the two concentrations agree for $M \sim 10^{14}\,h^{-1}{\rm M}_\odot$. Concentrations are very sensitive to the halo definition. In particular, at $z = 0$ values for $c_{\rm mean}$ are nearly twice as large as those for c_{200}. As expected, the difference becomes smaller at high redshift because the critical density will approach the mean density as the redshift becomes high enough for matter to dominate over vacuum energy. At $z = 0$ the median concentrations are typically about 10 per cent greater for the relaxed sample than for the default sample.

Using $C = 0$ and $M_{\rm pivot} = 10^{14}\,h^{-1}{\rm M}_\odot$, N07 found as the best fit for all NFW haloes in their $z = 0$ sample $(A_{200}, B_{200}) = (4.67, -0.11)$. Fitting the same function to our $z = 0$ sample gives $(A_{200}, B_{200}) = (3.93, -0.097)$ which yields concentrations that are lower by a factor ranging from 23 per cent at $10^{11}\,h^{-1}{\rm M}_\odot$ to 16 per cent at $10^{14}\,h^{-1}{\rm M}_\odot$. This difference can be attributed to the decrease in σ_8. If σ_8 is higher then haloes of a given mass form earlier. This increases the concentration because c reflects the background density of the universe at the time when the halo forms (NFW).

The scatter in the concentration about the median $c(M)$ relation has been shown to be lognormal for relaxed haloes (Jing 2000), with a slight decrease in the scatter as a function of mass (N07). The inclusion of unrelaxed haloes adds a tail towards low concentrations. Fig. 3 shows histograms of the $z = 0$ concentrations using both NFW (black) and Einasto (red) profiles for both the default (solid) and relaxed (dashed) samples. Either density profile yields a distribution which agrees qualitatively with that found by N07 for the NFW model. Fitting lognormal functions to the probability density functions yields $\sigma(\log_{10} c_{200}) = 0.15$ and 0.17 for the NFW and Einasto density profiles, respectively. For the relaxed sample the scatter is significantly smaller: $\sigma(\log_{10} c_{200}) = 0.11$ and 0.12.

Figure 4 compares our predictions with the observations of Buote et al. (2007) and Schmidt & Allen (2007), who measured NFW $c_{\rm vir}$ concentrations from X-ray observations of some 70 groups and clusters with a median redshift of $z = 0.1$. The observationally inferred concentrations are significantly greater than the predicted medians and the discrepancy increases with decreasing mass. Using only relaxed haloes (dashed lines) does not help much because it removes only the low-concentration tail. Observations and theory could be brought back into agreement if the predicted concentrations are too low, for example because gas physics has not been taken into account. Alternatively, the

[1] As a check of our analysis procedure, we ran and analysed a miniature version of the `MS` with identical mass and force resolution (we used a box of $50\,h^{-1}$Mpc on a side containing 216^3 particles) and were able to reproduce N07's result to within the errors.

Table 1. Best-fit parameters for the median $c(M, z)$ relation (Eq. 4) using $M_{\rm pivot} = 2 \times 10^{12}\, h^{-1}{\rm M}_{\odot}$ for three different halo definitions, two different density profiles, redshift $z = 0$ and $z = 0$–2 and for both the full (F) and relaxed (R) halo samples. The errors correspond to $1\,\sigma$ confidence intervals and have been determined by bootstrap resampling the haloes.

			NFW			Einasto	
Sample	Redshift	A_{200}	B_{200}	C_{200}	A_{200}	B_{200}	C_{200}
F	0	$5.74\pm^{0.12}_{0.12}$	$-0.097\pm^{0.006}_{0.006}$	0	$6.48\pm^{0.15}_{0.15}$	$-0.127\pm^{0.009}_{0.009}$	0
F	0–2	$5.71\pm^{0.12}_{0.12}$	$-0.084\pm^{0.006}_{0.006}$	$-0.47\pm^{0.04}_{0.04}$	$6.40\pm^{0.16}_{0.16}$	$-0.108\pm^{0.007}_{0.007}$	$-0.62\pm^{0.04}_{0.04}$
R	0	$6.67\pm^{0.11}_{0.11}$	$-0.092\pm^{0.007}_{0.007}$	0	$7.70\pm^{0.14}_{0.15}$	$-0.127\pm^{0.008}_{0.009}$	0
R	0–2	$6.71\pm^{0.12}_{0.12}$	$-0.091\pm^{0.009}_{0.009}$	$-0.44\pm^{0.05}_{0.05}$	$7.74\pm^{0.15}_{0.16}$	$-0.123\pm^{0.009}_{0.008}$	$-0.60\pm^{0.05}_{0.05}$
		$A_{\rm vir}$	$B_{\rm vir}$	$C_{\rm vir}$	$A_{\rm vir}$	$B_{\rm vir}$	$C_{\rm vir}$
F	0	$7.96\pm^{0.17}_{0.17}$	$-0.091\pm^{0.007}_{0.007}$	0	$9.03\pm^{0.23}_{0.23}$	$-0.122\pm^{0.008}_{0.009}$	0
F	0–2	$7.85\pm^{0.17}_{0.18}$	$-0.081\pm^{0.006}_{0.006}$	$-0.71\pm^{0.04}_{0.04}$	$8.82\pm^{0.23}_{0.24}$	$-0.106\pm^{0.007}_{0.007}$	$-0.87\pm^{0.05}_{0.05}$
R	0	$9.23\pm^{0.15}_{0.15}$	$-0.089\pm^{0.013}_{0.010}$	0	$10.79\pm^{0.18}_{0.19}$	$-0.125\pm^{0.008}_{0.009}$	0
R	0–2	$9.23\pm^{0.17}_{0.16}$	$-0.090\pm^{0.009}_{0.009}$	$-0.69\pm^{0.05}_{0.05}$	$10.77\pm^{0.21}_{0.21}$	$-0.124\pm^{0.008}_{0.008}$	$-0.87\pm^{0.06}_{0.05}$
		$A_{\rm mean}$	$B_{\rm mean}$	$C_{\rm mean}$	$A_{\rm mean}$	$B_{\rm mean}$	$C_{\rm mean}$
F	0	$10.39\pm^{0.22}_{0.22}$	$-0.089\pm^{0.006}_{0.007}$	0	$11.84\pm^{0.29}_{0.30}$	$-0.124\pm^{0.007}_{0.008}$	0
F	0–2	$10.14\pm^{0.22}_{0.23}$	$-0.081\pm^{0.006}_{0.006}$	$-1.01\pm^{0.04}_{0.04}$	$11.39\pm^{0.29}_{0.31}$	$-0.107\pm^{0.007}_{0.007}$	$-1.16\pm^{0.05}_{0.05}$
R	0	$12.00\pm^{0.18}_{0.19}$	$-0.087\pm^{0.012}_{0.010}$	0	$14.03\pm^{0.23}_{0.24}$	$-0.116\pm^{0.008}_{0.008}$	0
R	0–2	$11.93\pm^{0.21}_{0.21}$	$-0.090\pm^{0.009}_{0.009}$	$-0.99\pm^{0.05}_{0.05}$	$13.96\pm^{0.28}_{0.27}$	$-0.119\pm^{0.009}_{0.008}$	$-1.17\pm^{0.06}_{0.06}$

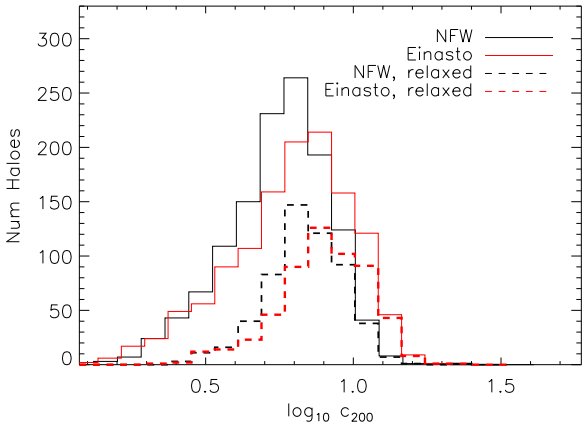

Figure 3. Histogram of halo concentrations using the NFW (black) and Einasto (red) density profiles for the default (solid) and relaxed (dashed) samples.

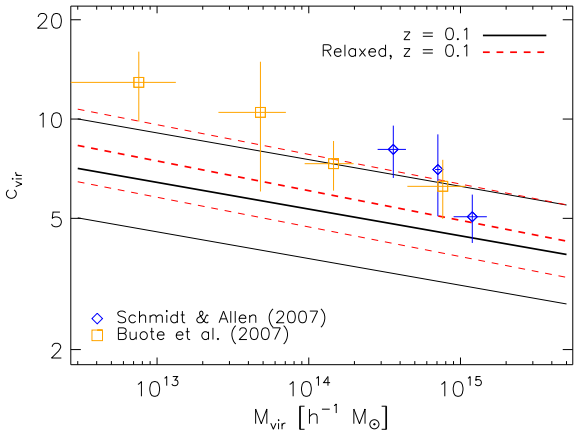

Figure 4. Comparison of observed and predicted NFW $c_{\rm vir}(M)$ relations at $z = 0.1$. Data points indicate weighted averages over about 10 objects taken from Buote et al. (2007) (squares) and Schmidt & Allen (2007) (diamonds). The sets of solid (dashed) lines are our predictions for the median concentrations and the $\pm 1\,\sigma$ lognormal scatter.

observed sample may be highly biased towards objects with high concentrations because these typically have higher X-ray luminosities, particularly for groups.

3.1 Comparison with predictions from the literature

A number of semi-empirical prescriptions (i.e. theoretically motivated fitting functions) have been proposed to predict the $c(M, z)$ relation for arbitrary cosmologies. The basic premise of each is that the concentration of a halo reflects the background density of the universe at the formation time of the halo. The prescriptions differ mainly in the definition of this formation time. We will compare our results to the prescriptions proposed by NFW and ENS.[2]

The NFW prescription for $c(M)$ has three free parameters. The first two, F and f, are used to define the collapse redshift as the redshift for which a fraction F of the final halo mass M is contained in progenitors of mass $\geqslant fM$. The third parameter, C, gives the ratio of $\delta_{\rm c}$, which is 1-1 related to the concentration parameter in the NFW prescription, and the mean density of the universe at the collapse redshift. The values initially suggested by NFW are (F, f,

[2] We also compared with Bullock et al. (2001), using the values of $K = 2.9$ and $F = 0.001$ (Wechsler et al. 2006) and found significant disagreement with our data at high masses (see Fig. 2).

$C) = (0.5, 0.01, 3000)$, but we find that the modified values (0.1, 0.01, 200) provide a much better fit to our default sample while the relaxed sample is best fit by (0.5, 0.01, 500) although the latter values are poorly constrained. Both the original and our modified prescriptions are compared to our data in Fig. 2. The modified NFW model reproduces the full sample of NFW halo concentrations over a wide range of masses and redshifts, while the original model strongly overestimates the concentrations at $z = 2$ (bottom panel).

The ENS prescription has only one free parameter, C_σ, which implicitly defines the collapse redshift through $D(z_c)\sigma_{\rm eff}(M_s) = 1/C_\sigma$, where $D(z)$ is the linear growth factor, $\sigma_{\rm eff}(M)$ is the effective amplitude of the linear power spectrum at $z = 0$ and $M_{\rm s} = M(r < 2.17r_{\rm s})$. The concentration then follows (iteratively) by equating the characteristic density $\rho_s = 3M/(4\pi r_s^3)$ to the spherical collapse top-hat density at the collapse epoch. ENS found that $C_\sigma = 28$ was a good fit, but G07 concluded that this did not describe their data very well (see also Zhao et al. 2003). We performed a χ^2 fit (equally weighting all points) and found $C_\sigma = 29$ and 30 as the best-fit values using NFW and Einasto density profiles, respectively. While the ENS prescription is an excellent fit for NFW density profiles below $z = 2$, it underestimates the $z = 0$ concentrations for $M < 10^{12}\,h^{-1}{\rm M}_\odot$ when the Einasto density profile is used.

4 CONCLUSIONS

We have measured the concentrations of DM haloes using three cosmological N-body simulations assuming the WMAP5 cosmology. We presented power-law relations between halo concentration and mass for $z = 0$ and $z = 0 - 2$ using both NFW and Einasto density profiles for three different halo definitions and we compared them to predictions from the literature. We found that halo concentrations are significantly lower in the WMAP5 cosmology than in the WMAP1 cosmology, which was used in the `Millennium Simulation`. For $z = 0$ the reduction varies from 23 per cent at $10^{11}\,h^{-1}{\rm M}_\odot$ to 16 per cent at $10^{14}\,h^{-1}{\rm M}_\odot$.

While the decrease in the concentrations may improve the agreement between models and observations of galaxies, we found that it results in significant discrepancies with X-ray observations of groups and clusters of galaxies. To determine the seriousness of this discrepancy, it will be necessary to carefully study possible observational selection biases as well as the effects of baryons on the halo concentrations.

ACKNOWLEDGEMENTS

We thank V. Springel for letting us use SUBFIND and J. Bullock, C. Power and especially L. Gao for helpful discussions. We gratefully acknowledge J. Navarro's help in the use of CHARDEN and CENS, which we used for the $c(M)$ prescriptions for NFW and ENS, respectively. The simulations were run on the Cosmology Machine at the Institute for Computational Cosmology in Durham as part of the Virgo Consortium research programme and on Stella, the LOFAR BlueGene/L system in Groningen. This work was supported by an STFC studentship, a Marie Curie ETS grant, an ESF Short Visit grant, and by Marie Curie Excellence Grant MEXT-CT-2004-014112.

REFERENCES

Alam S. M. K., Bullock J. S., Weinberg D. H., 2002, ApJ, 572, 34
Broadhurst, T. & Barkana, R., 2008, arXiv:0801.1875
Bryan, G. & Norman, M., 1998, ApJ, 495, 80
Bullock, J., Kolatt, T., Sigad, Y., Somerville, R., Kratsov, A., Klypin, A., Primack, J., & Dekel, A., 2001, MNRAS, 321, 559
Buote D. A., Gastaldello F., Humphrey P. J., Zappacosta L., Bullock J. S., Brighenti F., Mathews W. G., 2007, ApJ, 664, 123
Davis, M., Efstathiou, G., Frenk, C., & White, D., 1985, ApJ, 292, 371
Dolag K., Bartelmann M., Perrotta F., Baccigalupi C., Moscardini L., Meneghetti M., Tormen G., 2004, A&A, 416, 853
Einasto, J., 1965, Alma-Ata, 51, 87
Eke, R., Navarro, J., & Steinmetz, M., 2001, ApJ, 554, 114
Gao, L., Navarro, J., Cole, S., Frenk, C., White, S., Springel, V., Jenkins, A., & Neto, A., 2007, arXiv:0711.0746 (G07)
Gnedin O. Y., Weinberg D. H., Pizagno J., Prada F., Rix H.-W., 2007, ApJ, 671, 1115
Hayashi, E. & White, S., 2007, arXiv:0709.3933
Hennawi J. F., Dalal N., Bode P., Ostriker J. P., 2007, ApJ, 654, 714
Jing Y. P., 2000, ApJ, 535, 30
Komatsu, E., Dunkley, J., Nolta, M. R., et al., 2008, arXiv:0803.0547
Kuhlen M., Strigari L. E., Zentner A. R., Bullock J. S., Primack J. R., 2005, MNRAS, 357, 387
Maccio, A., Dutton, A., van den Bosch, F., Moore, B., Potter, D., & Stadel, J., 2007, MNRAS, 378, 55
Navarro, J., Frenk, C., & White, S., 1997, ApJ, 490, 493
Neto, A., Gao, L., Bett, P., Cole S., Navarro J.F., Frenk C.S., White S.D.M., Springel V., 2007, MNRAS, 381, 1450 (N07)
Percival, W., Baugh, C., J., B.-H., et al., 2001, MNRAS, 327, 1297
Power, C., Navarro, J., Jenkins, A., Frenk, C., White, S., Springel, V., Stadel, J., & Quinn, T., 2003, MNRAS, 338, 14
Reed, D., Bower, R., Frenk, C., Jenkins, A., & Theuns, T., 2007, MNRAS, 374, 2
Schmidt, R., & Allen, S., 2007, MNRAS, 379, 209
Seljak, U., & Zaldarriaga, M., 1996, ApJ, 469, 437
Shaw L. D., Weller J., Ostriker J. P., Bode P., 2006, ApJ, 646, 815
Spergel, D., Verde, L., Peiris, H., et al., 2003, ApJS, 148, 175
Springel, V., 2005, MNRAS, 364, 1105
Springel, V., White, S., Jenkins, A., et al., 2005, Nature, 435, 629
Springel, V., White, S. D. M., Tormen, G., & Kauffmann, G., 2001, MNRAS, 328, 726
van den Bosch F. C., Mo H. J., & Yang X., 2003, MNRAS, 345, 923

Wechsler R. H., Zentner A. R., Bullock J. S., Kravtsov A. V., Allgood B., 2006, ApJ, 652, 71
Zhao, D.H., Jing, Y.P., Mo, H.J., Borner, G., 2003, ApJ, 597, 9